Supporting Information

Walker et al. 10.1073/pnas.1714622115

SI Materials and Methods

HEK293-$(CAGA)_{12}$ Luciferase-Reporter Assay. Luciferase-reporter assays for activation and inhibition were performed as previously described (1–5). Briefly, HEK293 $(CAGA)_{12}$ cells (from RRID: CVCL_0045) stably transfected with plasmid containing Firefly luciferase-reporter gene under the control of SMAD3-responsive promoter were seeded in growth media at 20,000 cells per well in a 96-well poly-D-lysine–coated flat-bottom plate (655940; Greiner Bio-One GmbH) and incubated at 37 °C/5% CO_2 until 75–85% confluent. For transient expression experiments, 200 ng total DNA in a final volume of 25 μL (25–75 ng ligand DNA, 50 ng full-length human furin in pcDNA4, and 5–50 ng of appropriate TLD DNA in pRK5 or pcDNA3, filled to 200 ng with empty vector) per well was added directly to the growth media, incubated for 6 h, and exchanged into serum-free media. OPTI-MEM reduced serum media (31985-070; Gibco, Life Technologies) and TransIT-LT1 Reagent (MIR 2300; Mirus Bio LLC) were utilized for transfection according to manufacturer instructions. Cells were lysed 30 h posttransfection using 20 μL per well 1× Passive Lysis Buffer (E1941; Promega), on a plate shaker (800 rpm, 20 min, 20 °C). The lysates were transferred to opaque black and white 96-well plates, 40 μL of LAR (E1501 and E1960; Promega) was added, and Firefly luminescence was recorded on a Synergy H1 Hybrid Plate Reader (BioTek). When necessary, subsequent addition of 40 μL of Stop&Glo substrate (E1960; Promega) was added and Renilla luminescence was recorded. To determine EC_{50} and IC_{50} values, the growth media was removed and the appropriate dilutions of either ligand alone or with antagonist, respectively, were serially titrated and added to the cells in a 100-μL total volume of serum-free media. Luminescence was recorded as mentioned 18–24 h after ligand or antagonist addition. Experiments were independently performed at least two times and all data points were performed in triplicate. The EC_{50} and IC_{50} values were derived from nonlinear regression with variable slope using GraphPad Prism 5 software. The EC_{50} and IC_{50} mean and SE were calculated for each experiment and the mean weighted to the SE was calculated using the following formulas, where a is the SE of the EC_{50} or IC_{50} determination, and so on (6):

$$\text{weighted mean} = \frac{\left(\frac{A}{a^2}\right) + \left(\frac{B}{b^2}\right) + \dots}{\left(\frac{1}{a^2}\right) + \left(\frac{1}{b^2}\right) + \dots} \quad \text{[S1a]}$$

and

$$\text{weighted error} = \frac{\left(\frac{1}{a}\right) + \left(\frac{1}{b}\right) + \dots}{\left(\frac{1}{a^2}\right) + \left(\frac{1}{b^2}\right) + \dots}. \quad \text{[S1b]}$$

Production and Purification of GDF8 Prodomain from *E. coli*. The prodomain of human GDF8 (residues 24–262) was cloned into a modified pET28a expression vector that contains an N-terminal 6x histidine tag, MBP containing the mutations D82A/K83A/E172A/N173A/K239A for surface entropy reduction (7), and an HRV-3C protease cleavage site [6xHis-MBP-HRV3C cleavage site-GDF8 (residues 24–262)]. The cysteine residues in the human GDF8 prodomain (C39/C41/C137/C138) were mutated to serine to improve expression and solubility and were shown to form a stable complex with mature GDF8 similar to mammalian-derived GDF8 prodomain. *E. coli* Rosetta (DE3) strain carrying the appropriate prodomain construct was grown at 37 °C, 220 rpm until an OD of 0.8 at 600 nm was achieved, followed by cold induction with 0.5 mM IPTG, addition of 2% ethanol, and incubation at 20 °C overnight. Cells were lysed and soluble 6xHis-MBP-GDF8 prodomain was applied to a nickel affinity column (GE Lifesciences) equilibrated in 20 mM Tris, pH 7.4, and 500 mM NaCl followed by elution with a linear gradient using 20 mM Tris, pH 7.4, 500 mM NaCl, and 500 mM imidazole over five column volumes. The eluted protein was then dialyzed into 20 mM Tris, pH 7.4, and 500 mM NaCl and HRV-3C protease was added and incubated for 24 h to remove the 6xHis-MBP-fusion protein. Following cleavage, the protein was dialyzed into 10 mM HCl and applied to a C4 reverse phase column (Sepax) equilibrated in 0.1% TFA and 5% acetonitrile and eluted with a linear gradient to 0.1% TFA and 95% acetonitrile over 30 column volumes. The fractions containing GDF8 prodomain protein were pooled and buffer-exchanged into 10 mM HCl for storage at −80 °C for future use.

Mammalian-Derived Latent GDF8 Complex ($GDF8^L$) and Mutant Complexes. CHO cells stably producing GDF8 were used as previously described (1, 4, 5, 8, 9). Conditioned media containing GDF8 was concentrated ∼10-fold using tangential flow and buffer-exchanged into 50 mM Tris, pH 7.4, and 500 mM NaCl and applied to a Lentil Lectin-Sepharose 4B (Amersham Biosciences) column. Elution of GDF8 was conducted using the same buffer containing 500 mM methyl mannose followed by application to an S200 size-exclusion column (buffer 20 mM Hepes, pH 7.4, and 500 mM NaCl; Pharmacia Biotech). Molarity of the GDF8 latent complex was determined as previously described, using SDS/PAGE/Coomassie staining and the quantified GDF8 mature as a standard (5).

For the expression of mutant prodomain:GDF8 complexes, expi293 (Life Technologies) were transiently cotransfected with the pRK5 expression vector containing the mutant DNA and furin DNA. Conditioned medium was harvested 4 d posttransfection and applied to a Lentil Lectin-Sepharose 4B (Amersham Biosciences) column. Elution of the mutant prodomain:GDF8 complexes was conducted using the same buffer containing 500 mM methyl mannose followed by application to an SRT-SEC300 size-exclusion column (Sepax; buffer 20 mM Hepes, pH 7.4, and 500 mM NaCl). Molarity of the mutant complexes was determined as previously described, using SDS/PAGE/Coomassie staining and normalization to the mature dimer under nonreducing conditions (5).

SAXS. SAXS data were collected using the SIBYLS mail-in SAXS service. GDF8 latent complex was purified as described above with the exception that the protein was reapplied to a Phenomenex HPLC S2000 size-exclusion column equilibrated with 20 mM Hepes, pH 7.4, 500 mM NaCl, 1 mM EDTA, and 2% glycerol. Generation of the reformed GDF8 complex required separation of mature GDF8 from the prodomain using previously described methods (1, 4, 5, 8, 9). Briefly, following purification of the $GDF8^L$ complex, the complex was adjusted to 4 M guanidinium hydrochloride and 0.1% TFA and applied to a C4 reverse-phase column (Sepax). The fractions containing either the mature ligand or prodomain were then identified and quantified. The two proteins were then mixed together with an excess molar ratio of prodomain to mature ligand dimer (2.25 prodomain:1 ligand dimer) and neutralized with 100 mM Hepes, pH 7.4, and 500 mM NaCl. The protein was then applied to a Phenomenex HPLC S2000 size-exclusion column as described above. Fractions from each peak were analyzed using SDS/PAGE followed by Western analysis to ensure that both proteins were present. Acid activation

of $GDF8^{L}$ complex was performed as described above. Data were collected on purified at least two concentrations of $GDF8^{L}$, $GDF8^{AA}$, and $GDF8^{R}$ in 20 mM Hepes, pH 7.4, 500 mM NaCl, 1 mM EDTA, and 2% glycerol at 10 °C. Four exposure times of 0.5, 1, 2, and 5 s were collected. Exposures exhibiting radiation damage were discarded. Buffer matched controls were used for buffer subtraction. ScÅtter (SIBYLS) and the ATSAS program suite (EMBL) were used for data analysis. Comparison of the experimental scattering profiles to known crystal structures was performed using the FoXS webserver (10). Ab initio molecular envelopes were calculated using from the average of 23 independent DAMMIN (ATSAS, EMBL; ref. 11) runs using P2 symmetry, averaged using DAMAVER (ATSAS, EMBL; ref. 12), and filtered using DAMFILT (ATSAS, EMBL). SUPCOMB (ATSAS, EMBL; ref. 13) was used to superimpose the crystal structure of the latent GDF8 protein complex (14).

Western Analysis. To test protein expression following transfection, 500,000 HEK293 $(CAGA)_{12}$ cells mentioned above (from RRID: CVCL_0045) were plated in a six-well plate coated with poly-D lysine and incubated at 37 °C until 75–85% confluency. A mixture of 625 ng of GDF8 DNA, 1.25 μg of furin, and 3.125 μg of pRK5 EV was used, totaling 5 μg of DNA, ∼25× the DNA used in a 96-well to closely mimic conditions within our luciferase assay. OPTI-MEM reduced serum media (31985-070; Gibco, Life Technologies) and TransIT-LT1 Reagent (MIR 2300; Mirus Bio LLC) were utilized for transfection according to manufacturer instructions. Twelve hours posttransfection media was removed and replaced with serum-free media. Thirty hours posttransfection media was removed and concentrated 25× and run under reducing conditions on an SDS/PAGE gel. Standard western protocols were utilized and the anti-GDF8 antibody from RnD Biosystems (AF788) was used as described by the manufacturer. Western blot was developed using the SuperSignal West Pico detection reagent (Thermo Fisher) per manufacture instructions and detected using the C-DiGit blot scanner (LI-COR).

Production of AAV Vectors. The cDNA constructs encoding for WT GDF8, GDF8 I56E, and GDF8 H112A were cloned into an AAV expression plasmid consisting of a CMV promoter/enhancer and SV40 poly-A region flanked by AAV2 terminal repeats. These AAV plasmids were cotransfected with pDGM6 packaging plasmid into HEK293 cells to generate type-6 pseudotyped viral vectors. Briefly, HEK293 cells were seeded onto culture plates for 8–16 h before transfection. Plates were transfected with a vector-genome-containing plasmid and the packaging/helper plasmid pDGM6 by calcium phosphate precipitation. After 72 h, the media and cells were collected and subjected to three cycles of freeze–thaw followed by 0.22-μm clarification (Millipore). Vectors were purified from the clarified lysate by affinity chromatography using heparin columns (HiTrap; GE Healthcare), the eluent was ultracentrifuged overnight, and the vector-enriched pellet was resuspended in sterile physiological Ringer's solution. The purified vector preparations were quantified with a customized sequence-specific quantitative PCR-based reaction (Life Technologies).

Administration of AAV6 Vectors to Mice. All experiments were conducted in accordance with the relevant code of practice for the care and use of animals for scientific purposes (National Health & Medical Council of Australia, 2016). Vectors carrying transgenes of GDF8 mutants were injected into the right TA muscle of 6- to 8-wk-old male C57BL/6 mice under isoflurane anesthesia at 10^{10} vector genomes (vg). As controls, the left TA muscles were injected with AAVs carrying an empty vector at equivalent doses. At the experimental endpoint, mice were humanely killed via cervical dislocation, and TA muscles were excised rapidly and weighed before subsequent processing.

Histological Analysis. Harvested muscles were placed in OCT cryoprotectant and frozen in liquid nitrogen-cooled isopentane. The frozen samples were cryosectioned through the middle of the muscle at 10-μm thickness and stained with hematoxylin and eosin. All sections were mounted using DePeX mounting medium (VWR) and imaged at room temperature using a U-TV1X-2 camera mounted to an IX71 microscope, and an Olympus PlanC 10×/0.25 objective lens. DP2-BSW acquisition software (Olympus) was used to acquire images. Images were separated into eight fields covering the whole of the TA muscle (designated A1–A4 and B1–B4). The minimum Feret's diameter of muscle fibers in fields A2, B2, and B3 were determined using ImageJ software (NIH) by measuring at least 300 fibers per mouse muscle. The same fields were compared for each TA muscle examined.

1. Cash JN, et al. (2012) Structure of myostatin·follistatin-like 3: N-terminal domains of follistatin-type molecules exhibit alternate modes of binding. *J Biol Chem* 287:1043–1053.
2. Cash JN, Angerman EB, Keutmann HT, Thompson TB (2012) Characterization of follistatin-type domains and their contribution to myostatin and activin A antagonism. *Mol Endocrinol* 26:1167–1178.
3. Cash JN, et al. (2013) Development of a small-molecule screening method for inhibitors of cellular response to myostatin and activin A. *J Biomol Screen* 18:837–844.
4. Walker RG, et al. (2015) Alternative binding modes identified for growth and differentiation factor-associated serum protein (GASP) family antagonism of myostatin. *J Biol Chem* 290:7506–7516.
5. Walker RG, et al. (2017) Structural basis for potency differences between GDF8 and GDF11. *BMC Biol* 15:19.
6. Jones DC, et al. (2010) Identification of a κ-opioid agonist as a potent and selective lead for drug development against human African trypanosomiasis. *Biochem Pharmacol* 80:1478–1486.
7. Moon AF, Mueller GA, Zhong X, Pedersen LC (2010) A synergistic approach to protein crystallization: Combination of a fixed-arm carrier with surface entropy reduction. *Protein Sci* 19:901–913.
8. Cash JN, Rejon CA, McPherron AC, Bernard DJ, Thompson TB (2009) The structure of myostatin:follistatin 288: Insights into receptor utilization and heparin binding. *EMBO J* 28:2662–2676.
9. Lee Y-S, Lee S-J (2013) Regulation of GDF-11 and myostatin activity by GASP-1 and GASP-2. *Proc Natl Acad Sci USA* 110:E3713–E3722.
10. Schneidman-Duhovny D, Hammel M, Sali A (2010) FoXS: A web server for rapid computation and fitting of SAXS profiles. *Nucleic Acids Res* 38:W540–W544.
11. Svergun DI (1999) Restoring low resolution structure of biological macromolecules from solution scattering using simulated annealing. *Biophys J* 76:2879–2886.
12. Volkov VV, Svergun DI (2003) Uniqueness of ab initio shape determination in small-angle scattering. *J Appl Crystallogr* 36:860–864.
13. Kozin MB, Svergun DI (2001) Automated matching of high- and low-resolution structural models. *J Appl Crystallogr* 34:1–9.
14. Cotton TR, et al. (2017) Structure of the human pro-myostatin precursor and determinants of growth factor latency. bioRxiv:153403.

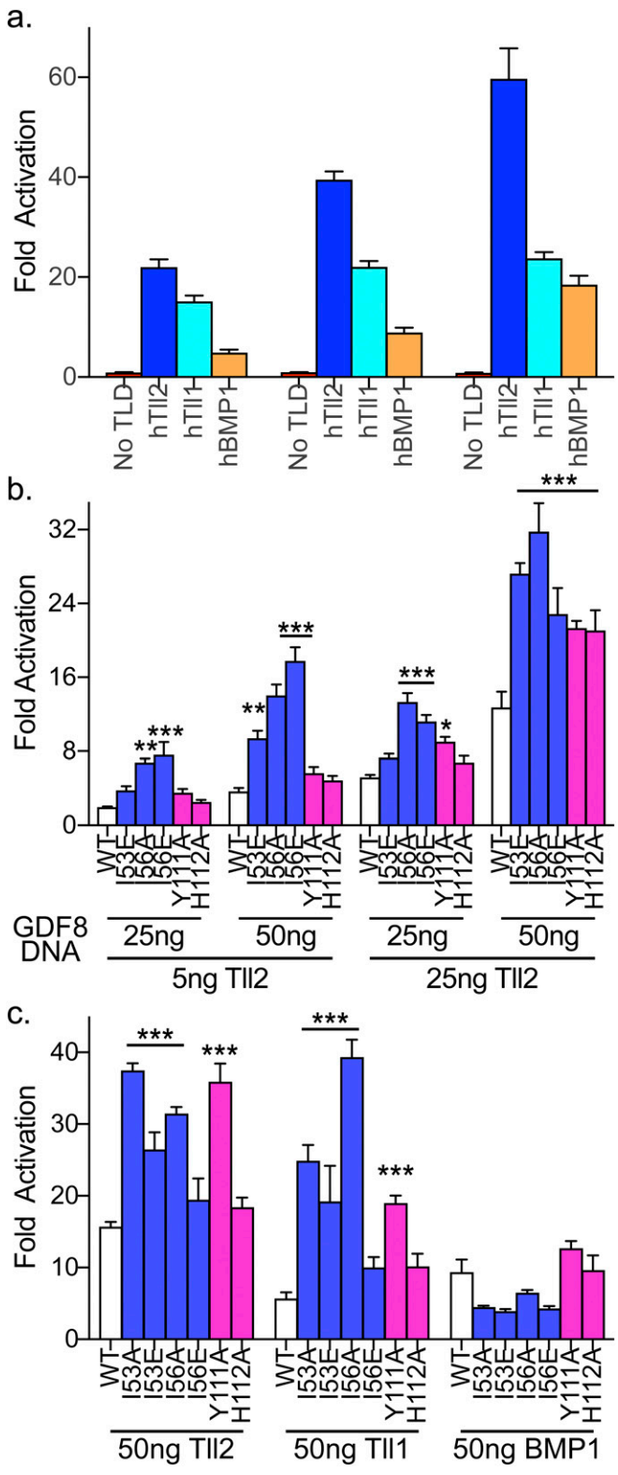

Fig. S1. (*A*) GDF8 activation by Tolloid. $(CAGA)_{12}$ HEK293 cells were cotransfected with varying amounts of GDF8 DNA within the pRK5 expression vector, 50 ng of furin (human), and 50 ng of Tll2, Tll1, or BMP1 (human). Media was exchanged for serum-free media 6 h posttransfection and luminescence was read 24 h later. The resulting luminescence was then divided by the signal from cells cotransfected with 50 ng of furin; 50 ng of Tll2, Tll1, or BMP1; and 25, 50, or 100 ng of pRK5 empty vector to report fold activation. (*B*) HEK293 $(CAGA)_{12}$ were cotransfected with 25 ng of the indicated GDF8 mutant in addition to 50 ng furin; 50 ng of Tll2, Tll1, or BMP1 DNA; and 25 ng of empty psF-IRES vector as a transfection control (Renilla). Duration of transfection and incubation before activity measurements was the same as in Fig. 3*B*. Luciferase signal was read first and then quenched followed by detection of Renilla. The luciferase signal for each well was normalized to the corresponding Renilla signal following normalization, the background signal from empty vector transfected wells, similar to Fig. 3*B*, was used to divide all samples to report fold activation (*C*), and GDF8 mutants were cloned into the psF-IRES vector and HEK293 $(CAGA)_{12}$ were cotransfected with 25 ng or 50 ng of DNA in addition to 50 ng of furin and 5 or 25 ng of Tll2. As in Fig. 3 *B* and *C* media was exchanged after 6 h and the plate read 24 h later. Signal was read and normalized as it was in *B*. Error is shown as mean ± SEM. Bar graphs were compared using two-way ANOVA with Bonferroni correction against WT (*$P \leq 0.05$, **$P \leq 0.01$, and ***$P \leq 0.001$).

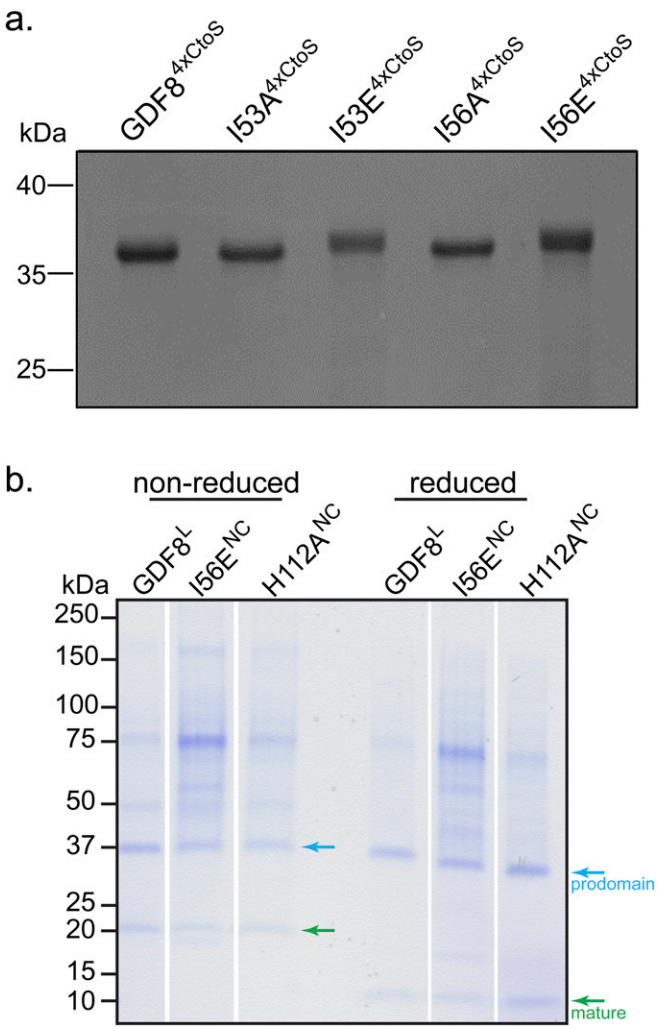

Fig. S2. Purification of bacterially produced GDF8 prodomains and mammalian-produced GDF8 prodomain complexes. (*A*) SDS gel of bacterially expressed and purified $GDF8^{4xCtoS}$ prodomain mutants. (*B*) GDF8 prodomain mutant complexes were purified from expi293F conditioned media using liquid chromatography. The Coomassie-stained SDS/PAGE gel depicts $GDF8^{L}$, $I56E^{NC}$, and $H112A^{NC}$ following purification using a Lentil Lectin-Sepharose B column followed by SEC in nonreducing and reducing conditions. The prodomain is shown by the blue arrow and the mature domain by the green arrow. Protein was normalized to mature dimer under nonreducing conditions using $GDF8^{L}$. Note that all proteins were run on the same gel that is shown here. For clarity purposes, the space in between some lanes is due to removal of gel lanes between samples pertinent to this study.

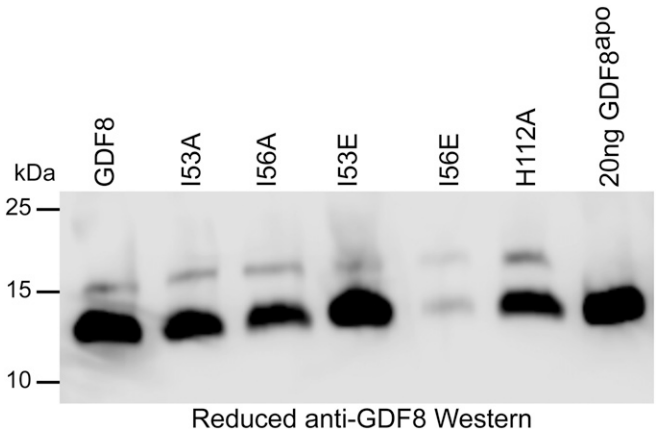

Fig. S3. Relative protein expression following transient transfection of various GDF8 prodomain mutant constructs. Conditioned media from $(CAGA)_{12}$ HEK293 cells was probed for mature GDF8 under reducing conditions to confirm expression within our luciferase assay.

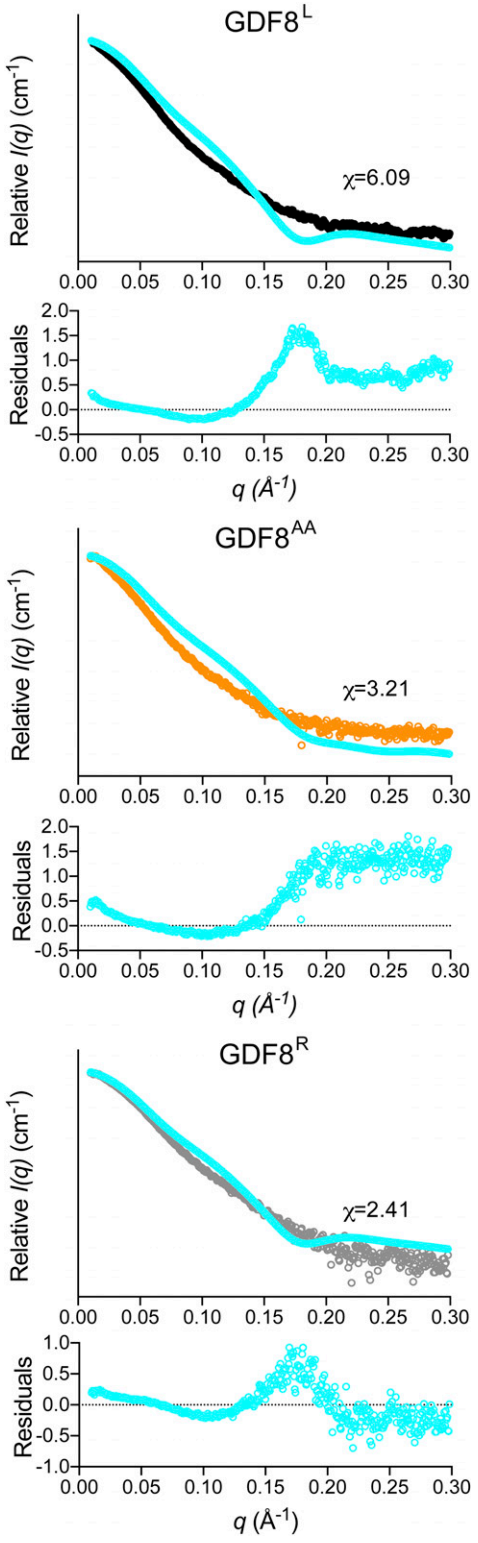

Fig. S4. Comparison of the experimental SAXS scattering profile of various GDF8 prodomain complexes to the GDF8 prodomain crystal structure. The panels show the theoretical scattering profile derived from the GDF8 prodomain complex crystal structure (cyan) compared with our experimental SAXS data on the various GDF8 prodomain complexes ($GDF8^{L}$: *Top*; $GDF8^{AA}$: *Middle*; $GDF8^{R}$: *Bottom*). The chi (χ) value, determined using FoXS webserver, for each comparison is shown adjacent to each scattering profile. The residuals for each comparison are shown below scattering profiles.

Table S1. Experimentally determined parameters from SAXS analysis of GDF8 prodomain complexes

Sample	Concentration, mg/mL	$I(0)$, cm^{-1}	R_g, Å		D_{max}, Å	Volume, $Å^3$	Mass, kDa
			Gunier	Real Space			
Native ($GDF8^{L}$)	3	4,400	41.7	39.3	136	310,000	90.0
	2	2,400	40.5	38.7	133	300,000	76.0
Acid-activated ($GDF8^{AA}$)	1.3	1,600	47.6	43.0	148	340,000	77.0
	1.15	1,700	47.0	41.6	147	350,000	70.0
	1	1,500	45.9	40.0	134	340,000	59.0
Reformed ($GDF8^{R}$)	1.6	190	40.0	39.0	131	270,000	89.0
Theoretical*							
proTGF-β1	NA	NA	28.5	NA	92	NA	82.4
proBMP9	NA	NA	37.8	NA	137	NA	90.2
proActivin A	NA	NA	31.6	NA	106	NA	90.1
proGDF8	NA	NA	34.9	NA	120	NA	80.1

NA, not assessed.
*Values derived from deposited PDB coordinates for each prodomain:ligand complex.

Table S2. Calculated IC_{50} values for various mutant GDF8 prodomain constructs

Construct	LogIC_{50} ± SEM, M	IC_{50}, nM	Log 95% CI, M	Fold over 4xCtoS
4xCtoS	−8.73 ± 0.02	1.85	−8.69 to −8.77	1.00
$GDF8^{4xCtoS}$ I53A	−8.42 ± 0.01	3.77	−8.39 to −8.46	2.04
$GDF8^{4xCtoS}$ I53E	−7.55 ± 0.01	28.27	−7.42 to −7.68	15.28
$GDF8^{4xCtoS}$ I56A	−8.56 ± 0.01	2.78	−8.52 to −8.59	1.50
$GDF8^{4xCtoS}$ I56E	−8.47 ± 0.01	3.35	−8.30 to −8.64	1.81
$GDF8^{4xCtoS}$ Y111A	−8.52 ± 0.02	3.01	−8.47 to −8.58	1.63
$GDF8^{4xCtoS}$ H112A	−8.58 ± 0.06	2.03	−8.53 to −8.60	1.10

Table S3. Calculated EC_{50} values for various mutant GDF8 prodomain constructs

Construct	LogEC_{50} ± SEM, M	EC_{50}, nM	Log 95% CI, M	Fold over $GDF8^{apo}$
$GDF8^{apo}$	−8.82 ± 0.03	1.53	−8.75 to -8.88	1.00
$GDF8^{L}$	NC	NC	NC	NC
$GDF8^{Native}$ I56E	−8.55 ± 0.06	2.79	−8.37 to -8.73	1.82
$GDF8^{Native}$ H112A	−7.86 ± 0.06	13.67	−7.70 to -8.03	8.93
$GDF8^{4xCtoS}$	−7.93 ± 0.02	10.62	−7.92 to -8.03	6.94
$GDF8^{4xCtoS}$ I53A	−9.23 ± 0.03	0.59	−8.90 to -9.57	0.39
$GDF8^{4xCtoS}$ I56A	−9.53 ± 0.06	0.30	−8.74 to -10.32	0.20
$GDF8^{4xCtoS}$ Y111A	−8.98 ± 0.09	1.05	−7.78 to -10.18	0.69

NC, not calculable.